Photoactivation of Chemotherapeutic Agents with Cerenkov Radiation for Chemo-Photodynamic Therapy

Uriel Gallaga-González, Enrique Morales-Avila, Eugenio Torres-García, José A. Estrada, Luis Enrique Díaz-Sánchez, German Izquierdo, Liliana Aranda-Lara,* and Keila Isaac-Olivé*

Read Online

ACCESS | Metrics & More | Article Recommendations

ABSTRACT: Cerenkov radiation (CR) can be used as an internal light source in photodynamic therapy (PDT). Methotrexate (MTX) and paclitaxel (PTX), chemotherapeutic agents with wide clinical use, have characteristics of photosensitizers (PS). This work evaluates the possibility of photoexciting MTX and PTX with CR from ^{18}F-FDG to produce reactive oxygen species (ROS) capable of inducing cytotoxicity. PTX did not produce ROS when excited by CR from ^{18}F-FDG, so it is not useful for PDT. In contrast, MTX produces $^1O_2$ (detected by ABMA) in amounts sufficient to significantly decrease the viability of the T47D cells. MTX solutions of 100 nM combined with ^{18}F-FDG activities of 50 (1.85 MBq) and 100 μCi (3.7 MBq) produced a significant decrease in cell viability to (50.09 ± 4.95) and $(47.96 \pm 11.19)\%$, respectively, compared to MTX $(66.29 \pm 5.92)\%$ and ^{18}F-FDG $(91.35 \pm 7.00\%$ for 50 μCi and $99.43 \pm 11.03\%$ for 100 μCi) alone. Using the CellRox Green reagent, the intracellular production of ROS was confirmed as the main mechanism of cytotoxicity. The results confirm the therapeutic potential of photoactivation with CR and the synergy of the combined treatment with chemotherapy + photodynamic therapy (CMT + PDT). The combination of chemotherapeutic agents with PS properties and β-emitting radiopharmaceuticals, previously approved for clinical use, will make it possible to shorten the evaluation stages of new CMT + PDT systems.
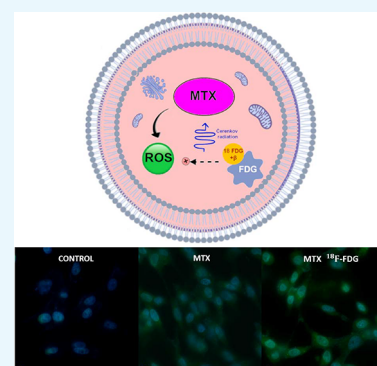
INTRODUCTION

The high incidence of cancer worldwide requires the continuous development, innovation, and implementation of increasingly efficient therapeutic strategies. Although chemotherapy (CMT) is widely applied in clinical practice, it has limitations, such as low therapeutic effects and systemic toxicity. Combining treatments, such as CMT + photodynamic therapy (PDT), produces a more effective synergistic therapeutic response than individual therapies.[1,2] For example, Sun et al. developed an aptamer@SPION nanosystem for co-delivering a chemotherapeutic agent and a photosensitizer molecule.[3] The significant decrease of cell growth under light irradiation of the nanosystem mainly resulted from the chemo-photodynamic synergistic effects.[3]

PDT is a therapeutic modality that uses light to excite photosensitive molecules (PS) accumulated in tumor tissue or its vasculature and produce reactive oxygen species (ROS), such as singlet oxygen ($^1O_2$) and superoxide anion (O_2^{*-}). ROS causes the oxidation of biomolecules, such as nucleic acids, lipids, and proteins, producing a severe alteration in cell signaling cascades or gene expression regulation. Depending on the type of cell, PS, light dose, and other variables, PDT can induce (a) cell death through different pathways (apoptosis, necrosis, autophagy), (b) vascular damage, (c) immune response, or a combination of these.[4−6]

When the PS in the ground state (^0PS) absorbs a light photon with appropriate energy, it is excited to a very unstable initial state called a singlet ($^1PS^*$). To de-excite, the $^1PS^*$ can emit light photons (fluorescence) or heat (internal conversion). It can also reverse the spin of the excited electron (intersystem crossing, ICS) and reach a more stable excited state called a triplet ($^3PS^*$). The $^3PS^*$ can go to the ^0PS state by (i) emitting light (phosphorescence), (ii) energy transfer to molecular oxygen (O_2) (type II reaction), or (iii) by electron or proton transfer to biomolecules or O_2 present in the tissue (type I reaction). When the type II reaction occurs, $^1O_2$ is formed, while the type I reaction produces free radicals that react with O_2 and form ROS, mainly the anionic radical O_2^{*-}, the precursor of H_2O_2 and the hydroxyl radical ($HO^\bullet$). All these species attack other molecules through a chain of reactions that are highly cytotoxic to cells.[4−8] Type I and II reactions occur simultaneously, but the proportion of occurrence of one or the other depends on various factors,

Methotrexate
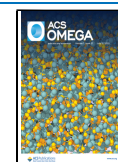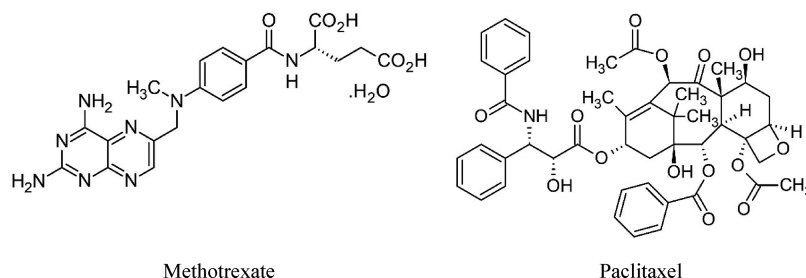
Paclitaxel

Figure 1. Chemical structures of methotrexate and paclitaxel.

for example, intrinsic characteristics of PS and the presence of different biomolecules and O_2 in the tissue.[5,6,9,10]

PDT has three important limitations: (1) low accumulation of PS in cancer cells, (2) O_2 shortage in hypoxic regions of the tumor, and (3) poor penetration of visible light into the tissue for the excitation energy range of many PSs.[8] This last limitation can be overcome if the PS and the light source are co-located within the cancer cells. One strategy to achieve the latter is to use Cerenkov radiation (CR) as an internal light source,[8,9] whose usefulness for PDT has been demonstrated by multiple authors.[11−14]

CR occurs when a charged particle, such as $\beta+$ or $\beta−$, travels through a dielectric medium at a speed greater than the speed of light in that medium ($v \geq c/n$, where n is the refractive index of the medium). The Cerenkov spectrum spans from 200 to 1000 nm and is most pronounced in the UV and blue regions, where many PSs absorb strongly.[8,14] For CR that occurs in biological tissue (refraction index $n \approx 1.4$), the energy of the charged particle must be greater than 250 keV.[9] This threshold is less than the energy of most β-particles emitting radio-nuclides, so almost all β-emitters produce CR. Once the threshold energy is exceeded, the shape of the Cerenkov spectrum is the same, but the intensity depends on the energy of the charged particle: the higher the energy, the higher the intensity;[8,15] hence, the CR intensity decreases in the order $^{90}Y > ^{68}Ga > ^{124}I > ^{89}Zr > ^{18}F > ^{64}Cu > ^{177}Lu$.[9,14]

Fluorodeoxyglucose labeled with ^{18}F (^{18}F-FDG) is a radiopharmaceutical (RF) widely used clinically for the diagnosis of tumors by nuclear imaging due to its high accumulation in tumor cells compared to healthy cells. Due to the nuclear characteristics of ^{18}F (97% β + emission of 635 keV of energy), ^{18}F-FDG has also been used to produce a photodynamic effect in the presence of different PSs.[8−10,12−14]

PS features are crucial in PDT. The PS must have a high degree of chemical purity, stability at room temperature, selectivity for cancer tissues, non-toxicity in the absence of light, and high quantum yield for the formation of the $^3PS^*$ state, excitation in a range of wavelengths (λ) that guarantees the penetration of light into the tissue, low cost, and easy availability, and $^3PS^*$ half-life should be sufficient to react with the surrounding molecules.[4,7,10] Although various PSs have been evaluated for use in PDT, very few reach clinical use. Using chemotherapeutic agents approved for clinical use such as PSs would reduce the time of preclinical research. Recent studies show that doxorubicin (DOX) produces ROS when irradiated with a 450 nm laser light and with CR from ^{18}F-FDG.[13] This evidence suggests that it is possible to use ^{18}F-FDG as a CR source to produce a photodynamic effect with other chemotherapeutic agents commonly used that present the same characteristics as PS.

The acid 2,4-diamine-4-deoxy-N10-metilpteroil glutamic (Metotrexato, MTX) and the benzoate ($2\alpha,4\alpha,5\beta,7\beta,10\beta,13\alpha$)-4,10-bis(acetyloxy)-13-{[(2R,3S)-3-(benzoylamino)-2-hydroxy-3-phenylpropanoyl]oxy}-1,7-dihy-droxy-9-oxo-5,20-epoxytax-11-en-2-yl (Paclitaxel, PTX) are chemotherapeutic agents widely used in clinical practice that show some PS characteristics.[16,17] Both molecules show high tropism toward tumor cells and have absorption, excitation, and emission spectra[16,17] in the region of the Cerenkov spectrum, so it is possible that they can be excited by CR from of ^{18}F-FDG and produce ROS. In this way, the cytotoxicity induced by both chemotherapeutic agents could be increased by using the combined effect of CMT+ PDT.

This work aimed to evaluate if the irradiation of MTX and PTX with CR from ^{18}F-FDG can produce ROS, particularly $^1O_2$ and $O_2^{*−}$, in concentrations sufficient to achieve a CMT + PDT effect. For the detection of ROS, the reagents 9,10-anthracenediyl-bis(methylene) dimalonic acid (ABMA) and 2,6-dichlorophenolindophenol (DCPIP) were used. The ABMA is widely used to estimate the formation of $^1O_2$,[6,13] while the DCPIP is an electron acceptor used to estimate the presence of $O_2^{*−}$.[13,18,19]

■ RESULTS AND DISCUSSION

MTX and PTX Irradiation with Increasing Activities of ^{18}F-FDG. Figure 1 shows that MTX is a molecule like folic acid composed of a diamino-pterin ring bound to a p-amino benzoyl moiety linked, in turn, to glutamic acid. Under the action of UV−vis light, it dissociates into p-aminobenzoyl glutamic acid and 2,4-diamino-6-formylpterin, which is highly fluorescent.[20,21] The degradation of MTX by the action of the UV−vis light can be monitored by the degradation of its 360 nm absorption band[22,23] or by the increase in the 470 nm emission band of pterin.[21] PTX, on the other hand, also shown in Figure 1, is a tetracyclic diterpenoid with a very complex structure in which a hydrocarbon skeleton formed by three cycles of six, eight, and six polysubstituted with four methyls and eight oxygenated functions stands out. The molecule has a total of 11 stereocenters[24] and shows slight fluorescent properties when excited with a 308 nm laser.[16] It can also be easily determined by UV spectroscopy.[22]

For a photodynamic effect to occur, it is necessary that the photons that hit the PS have enough energy ($1/\lambda^2$) to activate them. To find out if CR from ^{18}F-FDG could be capable of photoactivating MTX and PTX, the absorption spectra of MTX dissolved in water (water blank) and PTX dissolved in DMSO (DMSO blank) were obtained in the range of 250−500 nm and were superimposed with the Cerenkov emission spectrum of ^{18}F in the same range of wavelengths, constructed mathematically from the following equation:

$$\int_{250}^{500} f_1(\lambda)\,d\lambda$$

where $f_1(\lambda)$ is the function that describes the photon production for ^{18}F in the range of 250−500 nm and is defined as $f_1(\lambda) = 8.1704 \times 10^{-9}\lambda^3 + 1.5288 \times 10^{-5}\lambda^2 + 0.00769\lambda - 0.4379$.[25]

The CR from ^{18}F-FDG must be capable of photoactivating both chemotherapeutic agents due to their PS properties (Figure 2). The intensity of the Cerenkov spectrum at the λ
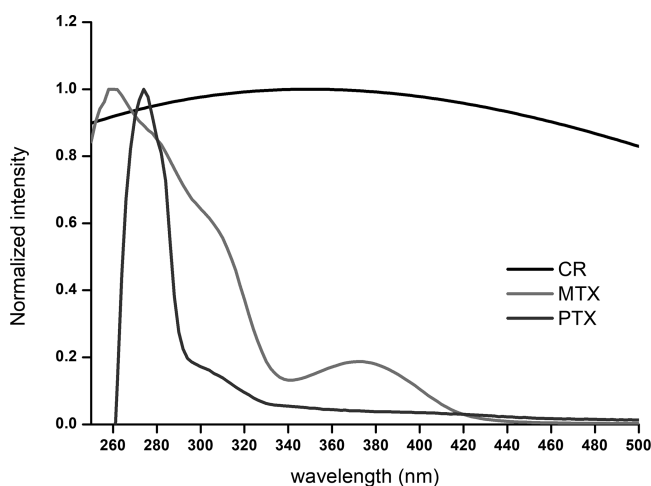
Figure 2. UV−vis spectra of MTX and PTX in the 250−500 nm range superimposed with the Cerenkov emission spectrum of ^{18}F-FDG.

absorption maxima of PTX (275 nm, GENESYS 50 UV−vis spectrophotometer, Thermo Fisher Scientific) and MTX (375 nm, Epoch UV−vis microplate reader, Biotek) seems adequate for this purpose. PS photoactivation induces degradation (photobleaching) due to the oxidation caused by ROS formation through type I and II reactions, decreasing its optical activity.[26,27] The efficiency of PDT can be evaluated *a priori*, by PS photobleaching, since the higher PS photobleaching, the lower the proportion of ROS available to induce cytotoxicity. The loss of the optical properties of PS facilitates the evaluation of photobleaching by decreasing absorbance.[13,26,27]

When we combined 200 μM aqueous solution of MTX with different activities of ^{18}F-FDG such as 250 (9.25 MBq), 500 (18.5 MBq), and 750 μCi (27.75 MBq), the 375 nm absorption band of the MTX slightly decreased with the ^{18}F-FDG activity increase (Figure 3A). This decrease is not very pronounced, which is in the range of 350−450 nm (Figure 3B). When plotting the absorbance values at 375 nm vs ^{18}F-FDG activity (Figure 3C), a straight line with almost zero slopes ($m = -6.23 \times 10^{-5}$) is obtained. This result may be due to low ROS formation, high MTX photostability, or both. Since MTX has PS-like properties,[17] the decrease in absorbance (Figure 3C) is most likely due to the interaction of the CR of ^{18}F-FDG with the pterin group of MTX to produce $^1O_2$, one of the main causes of PS photobleaching.[26] Pterin groups easily form $^1O_2$ in aerobic environments.[20]

The analysis of the values obtained at each point (Figure 3D) reveals that the absorbance value at 250 μCi (9.25 MBq) of ^{18}F-FDG (absorbance = 0.269) is part of the confidence interval of the first point (0.261−0.297), which corresponds to

0 μCi of ^{18}F-FDG. This indicates that it cannot be affirmed that a significant change in the absorbance of the MTX has occurred. The same result is obtained when analyzing the rest of the points, so it is concluded that, although $^1O_2$ should have been produced given the experiment conditions, the low Cerenkov photon yield of ^{18}F-FDG (1.32 photons /mm/ disintegration[9]), and high photostability of MTX, it is not possible to appreciate significant photobleaching.

A similar experiment, but with a 200 μM solution of PTX in DMSO, produced the results shown in Figure 4. A proportional decrease in the absorbance of the 258−264 nm band of PTX can be seen as ^{18}F-FDG activity increases (Figure 4A). The observed absorption decreases with 500 (18.5 MBq) and 750 μCi (27.75 MBq) were significant (Figure 4C).

The slope of the straight line obtained ($m = -5.36 \times 10^{-4}$, Figure 4B) is one order higher than that obtained by irradiating MTX, which may reveal greater production of ROS and/or lower photostability of PTX in relation to MTX. This lower photostability could be related to the higher number of unsaturated cyclic structures of PTX with respect to MTX. ROS, particularly $^1O_2$, tends to interact easily with unsaturated cyclic structures, causing irreversible damage to the molecules.[26] It is noteworthy that while the 258−264 nm band of PTX decreased with increasing activities of ^{18}F-FDG, the absorbance of the 300 nm band showed a slight increase. This could be related to the formation of some chemical species that, we hypothesize, could be the (i) product of PTX decomposition by the photoreaction with CR of ^{18}F-FDG, (ii) product of DMSO radiolysis caused by β^+ radiation of ^{18}F-FDG[28] whose sulfoxide group is very unstable against ionizing radiation,[29] or (iii) product of interactions of the excited PTX with itself and with DMSO due to radiolysis.[30] Like photoreactions, radiolysis induces the formation of free radicals and ROS that cause changes in the components of the solutions. In either case, the chemical species formed could also contribute to PTX photobleaching.[26] The appearance of a new band in the spectrum of the product was not observed in MTX. However, both experiments reveal that MTX and PTX do not show significant photobleaching in the presence of ^{18}F-FDG, which is very convenient for their possible use as PS in PDT using the CR of ^{18}F-FDG as a light source since that high photobleaching is undesirable in a PS.[4,7]

Spectrophotometric Estimation of the Presence of $^1O_2$ in Solutions of MTX and PTX Irradiated with ^{18}F-FDG. $^1O_2$ is the lowest excited electronic state of O_2. It plays a major role in the efficacy of PDT *in vivo* as it can (i) cause cell death directly through oxidative reactions in biological macromolecules, such as lipids, proteins, or DNA; (ii) damage the vasculature associated with the tumor; and (iii) activate the immune response against the tumor.[4−6] For the evaluation of a potential PS for PDT, it is important to estimate its capacity to produce $^1O_2$, the main cytotoxin in PDT. Although PS photobleaching is mainly caused by $^1O_2$, it also depends on other reactions in which $^1O_2$ is not involved,[26,27] so a specific method must be used to assess $^1O_2$ production independent of photobleaching. $^1O_2$ can be estimated directly by emission at 1270 nm or indirectly from its interaction with a sensitive substance whose structural changes are proportional to the concentration of $^1O_2$ in the medium. Depending on the nature of the sensor molecule, these structure changes can be monitored by different spectroscopic techniques such as NMR, ESR (also known as EPR), fluorescence, and UV−vis absorption.[6]
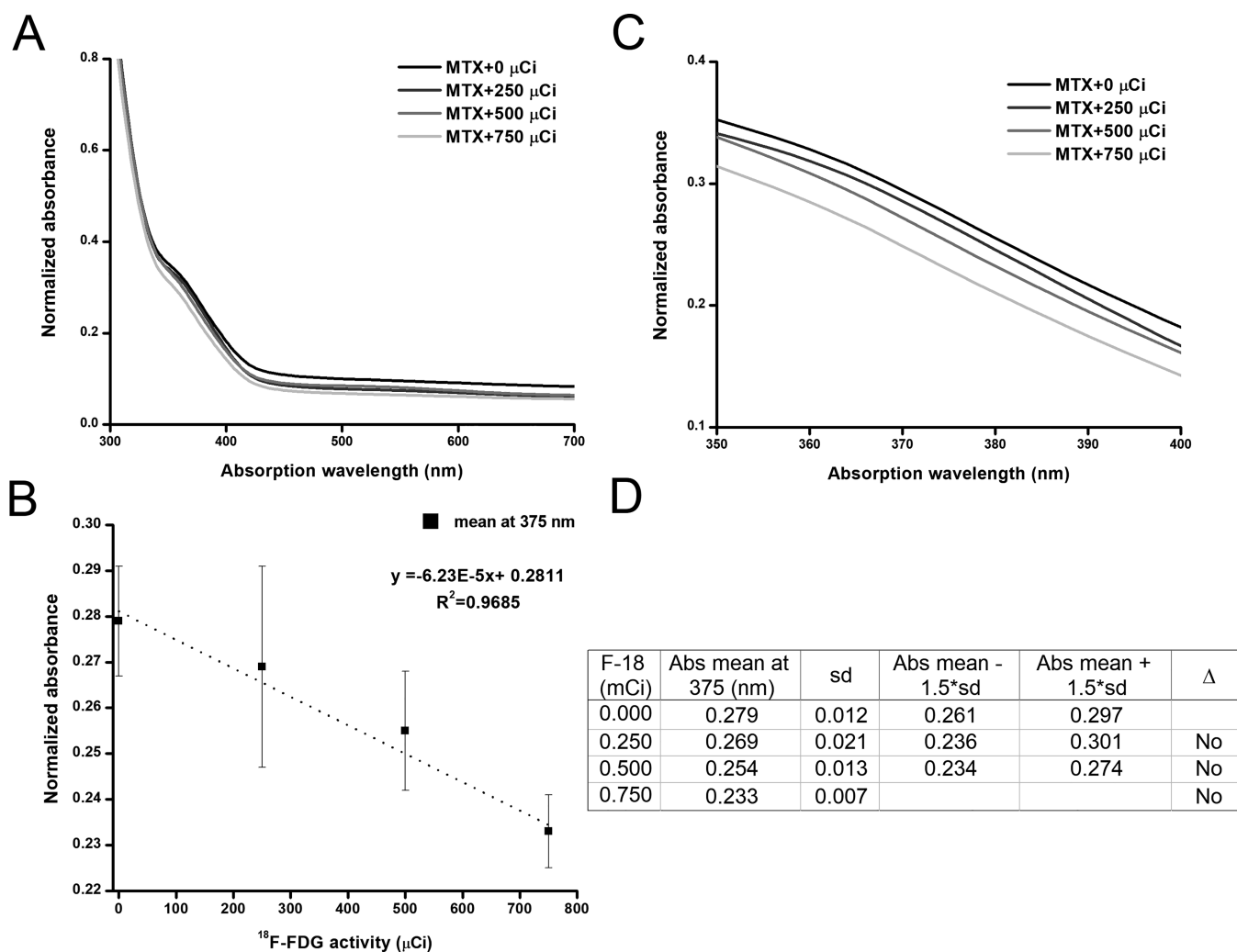
Figure 3. MTX absorption with different ^{18}F-FDG activities in the 300−700 nm range (A), MTX absorption in the 350−400 nm range with different ^{18}F-FDG activities (B). When plotting the absorbance of MTX at 375 nm vs ^{18}F-FDG activity (C), a straight line with almost zero slopes (-6.23×10^{-5}) is obtained, whose values are analyzed in the table (D).

To estimate the presence of $^1O_2$ by UV−vis spectrophotometry, ABMA was used, an anthracene derivative that reacts selectively with $^1O_2$, forming a non-fluorescent 9,10-endoperoxide (ABMA-O_2). ABMA-O_2 formation can be monitored spectrophotometrically by decreasing the absorption bands near 378 and 400 nm of ABMA.[6,13,15,31] When ABMA-O_2 is formed, the absorption of ABMA decreases proportionally to the amount of $^1O_2$ generated by the type II photodynamic reaction.[6,13,31] The decrease in ABMA absorption once $^1O_2$ was produced is irreversible. Therefore, this method is convenient when CR is used as light source because it allows the measurement of ABMA absorbance after ^{18}F-FDG total decay, avoiding the handle of the radioactive sample. Direct methods for $^1O_2$ determination, such as ESR, are sometime preferred over indirect methods, but in this case, it would have mean carrying out the $^1O_2$ measurement while sample was still radioactive.

Before determining the presence of $^1O_2$ in ABMA+MTX solutions, the behavior of ABMA against increasing activities of ^{18}F-FDG was evaluated, the results of which are shown in Figure 5. As can be seen, 250 μCi (9.25 MBq) of ^{18}F-FDG produces an appreciable decrease in the absorbance of the bands of 378−380 (Figure 5A,B) and 400−402 nm (Figure

5A,C) of ABMA, which then remains stable when adding higher activities of ^{18}F-FDG. This result indicates that the decrease in ABMA absorbance upon the addition of 250 μCi (9.25 MBq) of ^{18}F-FDG is unlikely to be a product of radiolysis since the signal was not affected by activities of 500 (18.5 MBq) and 750 μCi (27.75 MBq) of ^{18}F-FDG. We hypothesize that CR from ^{18}F-FDG is more likely to cause ABMA excitation to a state (probably triplet, according to Yin et al.[31]) in which it absorbs fewer photons without breaking down. As the amount of ABMA in the solutions is constant, increasing the intensity of the CR of ^{18}F-FDG does not increase the amount of excited ABMA, so the absorbance remains almost constant.

This behavior of ABMA in the face of increasing activities of ^{18}F-FDG is convenient for the determination of $^1O_2$ in MTX and PTX solutions since a decrease in the absorbance of these bands (different from that observed in Figure 4) would indicate the presence of $^1O_2$, given its selective reaction with ABMA.

When combining MTX with ABMA and different activities of ^{18}F-FDG (Figure 6), the intensity of the ABMA absorption bands decreased appreciably with the increase in the intensity of CR from ^{18}F-FDG (Figure 6A), which reveals the presence
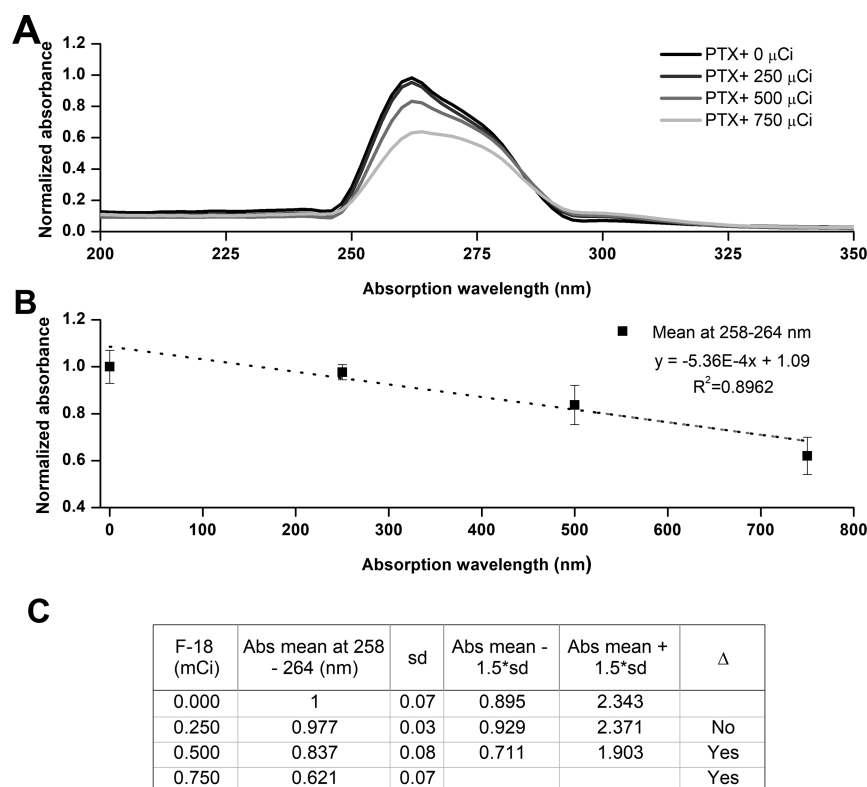
Figure 4. PTX absorption with different activities of ^{18}F-FDG in the range of 200−350 nm (A). When plotting the PTX absorbance at 258−254 nm vs ^{18}F-FDG activity, the line shown in (B) is obtained, whose values are detailed in the table (C).

of $^1O_2$. When plotting the variation of the absorbance of the 379 (Figure 6B) and 400 nm (Figure 6C) bands of ABMA (50 μM) in the presence of MTX (200 μM) and increasing activities of ^{18}F-FDG, it is clearly observed that the intensity of the ABMA bands decreases proportionally to the activity of ^{18}F-FDG, a phenomenon that was not observed in the solutions of ABMA+^{18}F-FDG in the absence of MTX (Figure 5). This decrease, whose analysis is shown in Figure 6D,E, is due to the reaction between ABMA with $^1O_2$ formed by the photoreaction that CR of ^{18}F-FDG induces on MTX with the consequent formation of ABMA-O_2. The slope of the line obtained at 379 nm ($m = -7 \times 10^{-4}$) is greater than that found at 400−401 nm ($m = -4 \times 10^{-4}$) because, at 379 nm, there is a greater contribution to the absorbance signal of the MTX than at 400 nm (Figure 6A), so some authors recommend using the band closest to 382 nm.[6] It has been found that although ^{18}F-CR produces a relatively small amount of $^1O_2$ molecules when porphyrin is used as PS, this amount is sufficient to cause cell damage, even at low ^{18}F-FDG activities due not only to the presence of $^1O_2$ but also to other species that are formed in the process.[9]

The fluorescent properties of PTX are weak (Motlagh et al.[16]). Adding increasing amounts of ^{18}F-FDG to solutions of PTX (200 μM) + ABMA (50 μM) did not produce the expected proportional decrease in ABMA absorbance (Figure 7A). However, a significant bathochromic shift of the entire spectrum was observed (Figure 7A), whose intensity increased in the presence of 250 μCi (9.25 MBq) of ^{18}F-FDG (Figures 7A−C) and then remained practically constant (Figure 7D,E), indicating that there was no formation of $^1O_2$. Since PTX photobleaching had initially been detected (Figure 4), this photobleaching is likely due to physicochemical trans-

formations in PTX solution in DMSO induced both by Cerenkov photons and by β + radiation from ^{18}F-FDG, which, although not associated with the presence of $^1O_2$, cause changes in the PTX spectrum, including the increase in the 300 nm band observed in Figure 3.

Estimation of the Presence of O_2*^- in Solutions of MTX and PTX Irradiated with ^{18}F-FDG by UV−Vis Spectrophotometry with DCPIP. Some authors have proposed that the efficacy of PDT should be evaluated only through the production of $^1O_2$.[9] However, there is evidence that the radical anion O_2*^- also contributes to the efficacy of PDT.[4,10] O_2*^- is not toxic by itself, but it is a precursor of H_2O_2 and $HO^\bullet$, with the latter considered the most cytotoxic ROS that exists.[32] O_2*^- is produced by a complex process when $^3PS*$ interacts with a biological substrate (type I reaction) and is reduced, and the reduced form reacts with O_2.[4,7,10,13] The reaction can also occur with free radicals and DNA.[10] The O_2*^- formed can be dismutated or undergo a second reduction and form H_2O_2, which, when it is reduced, gives rise to $HO^\bullet$. The presence of O_2*^- can be estimated indirectly by the decrease in the 600 nm band of electron acceptor DCPIP that decolorizes in O_2*^- presence.[10,13] First, the influence of ^{18}F-FDG radiation on DCPIP was determined. As shown in Figure 8A, increasing the activity of ^{18}F-FDG decreases the absorbance of the 586−604 nm band of DCPIP. When plotting the variation of absorbance as a function of ^{18}F-FDG activity (Figure 8B), similar to ABMA (Figure 5), the decomposition rate of DCPIP was not proportional to the concentration of ^{18}F-FDG. The reagent decomposes appreciably on the addition of 250 μCi (9.25 MBq) ^{18}F-FDG, but decomposition is slower after that.

When a solution of DCPIP (140 μM) + MTX (200 μM) is brought into contact with increasing activities of ^{18}F-FDG, a
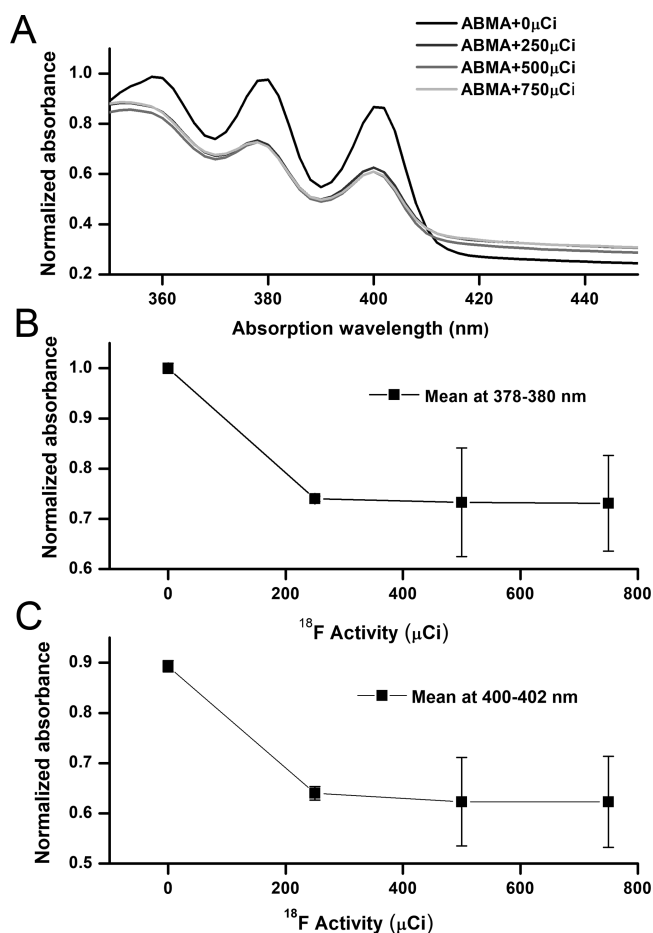
Figure 5. Irradiation of an aqueous solution (50 μM) of ABMA with different activities of ^{18}F-FDG. (A) ABMA absorption spectrum in the 350−450 nm range. (B) Variation of the absorbance of the 378−380 nm band of ABMA as a function of ^{18}F-FDG activity. (C) Variation of the absorbance of the 400−402 nm band of ABMA as a function of ^{18}F-FDG activity.

proportional decrease in the absorbance of the band (593−604 nm) of DCPIP is observed in the presence of increasing activities of ^{18}F-FDG (Figure 9A,B). However, the variation analysis shows that this decrease is lower than that obtained by irradiating DCPIP (Figure 8), so it is not possible to state that it is due to the presence of the O_2^{*-} radical. Unlike ABMA, DCPIP is very unstable in aqueous solutions. In the presence of O_2, it undergoes both oxidation and reduction reactions,[19] so it is likely to be more sensitive than ABMA to the interactions induced by β^+ radiation of ^{18}F-FDG.

To determine if PTX is capable of producing O_2^{*-} by type I reaction induced by CR of ^{18}F-FDG, we used solutions of DCPIP (140 μM) with PTX (200 μM) and different activities of ^{18}F-FDG. As shown in Figure 10, exposure of PTX to CR in the presence of DCPIP did not produce a significant decrease in the characteristic 600 nm absorption band of DCPIP as a function of increased ^{18}F-FDG activity.

The slope of the straight line obtained is almost zero ($m = -8 \times 10^{-5}$), as can be seen in Figure 10B and in the analysis of Figure 10C. Although it is very likely that O_2^{*-} was produced, given the chemical structure of PTX, its concentration was negligible. Since PTX did not form detectable amounts of $^1O_2$ or sufficient O_2^{*-} in the presence of increasing amounts of ^{18}F-

FDG, its evaluation in subsequent experiments was disregarded.

The lower photodegradation of MTX with respect to PTX (slopes -6.23×10^{-5} and -5.36×10^{-4} respectively), the appearance of a band at 300 nm in PTX, and the production of ROS by MTX and not by PTX indicate that an ICS process occurred in MTX that gave rise to transfer reactions, which did not occur in PTX. The results indicate that the interaction of CR or beta radiation from ^{18}F, or both, with PTX produces other chemical/photochemical processes not involved in ROS production.

Irradiation of MTX + ABMA and MTX + DCPIP Solutions with 250 μCi (92.5 MBq) of ^{18}F-FDG. To confirm the production of $^1O_2$ and O_2^{*-} when irradiating MTX with CR from ^{18}F-FDG, an additional experiment was carried but varying the concentration of MTX in solution (200, 400, 600, and 800 μM), keeping constant the concentration of ABMA (200 μM) or DCPIP (140 μM) and the activity of ^{18}F-FDG (250 μCi, 92.5 MBq). Figure 11 shows the results obtained with the ABMA, and Figure 12 shows those obtained with the DCPIP. As the concentration of MTX in the solution increases, the MTX + ABMA solutions absorbance increases (Figure 11) since both products absorb in the 350−400 nm region. However, the bands corresponding to ABMA (378−380 and 400−402 nm) practically disappear, in particular, the 400−403 nm band where the contribution of MTX is lower. As the concentration of MTX increases, the amount of $^1O_2$ that can react with ABMA to produce ABMA-O_2 increases. Since the concentration of ABMA is constant as more $^1O_2$ is produced, the ABMA is depleted. The increase in absorbance that is observed is due to the increase in the concentration of MTX. Given the disappearance of the ABMA bands, it was impossible to carry out a detailed analysis of the behavior of the solutions as in the previous cases.

Figure 12, however, reveals a different behavior of the MTX + DCPIP solutions. A proportional variation of the absorbance of the 592−598 nm band of DCPIP was not observed as a function of the MTX concentration but rather a random behavior (Figure 12B). The values obtained in all the concentrations of MTX studied are included in the range of signal variation in the absence of MTX (Figure 12C), confirming that the radical anion O_2^{*-} is not formed.

These results reveal that in the presence of O_2, MTX can produce $^1O_2$ through a type II reaction from the photoexcitation induced by CR from ^{18}F-FDG. This behavior facilitates the design of a hybrid CMT + PDT system in which MTX acts in unison as a chemotherapeutic and photosensitizer.

Intracellular Evaluation of ROS. The location of the PS, inside or on the cell surface, is essential in PDT.[4,7] When CR is used as an excitation source, it is most convenient for both the PS and the radionuclide to be located intracellularly. $^1O_2$ has a short lifetime (0.01−0.04 μs), so its path in the cell is short (10−55 nm).[6,7] The average path of ^{18}F-FDG β^+ particles is 600 nm.[33] Therefore, to produce an appreciable photodynamic effect by MTX + ^{18}FDG combination, it is convenient to produce $^1O_2$ inside the cell. MTX enters the cell by two mechanisms: active transport and passive diffusion. Active transport via the reduced folate transporter (RFC) and folate receptors present on the cell membrane is the dominant mechanism.[34,35] ^{18}F-FDG enters cells through glucose transporters (GLUT), and once it is phosphorylated by glucose 6-hexokinase, it remains trapped inside it, accumulating propor-
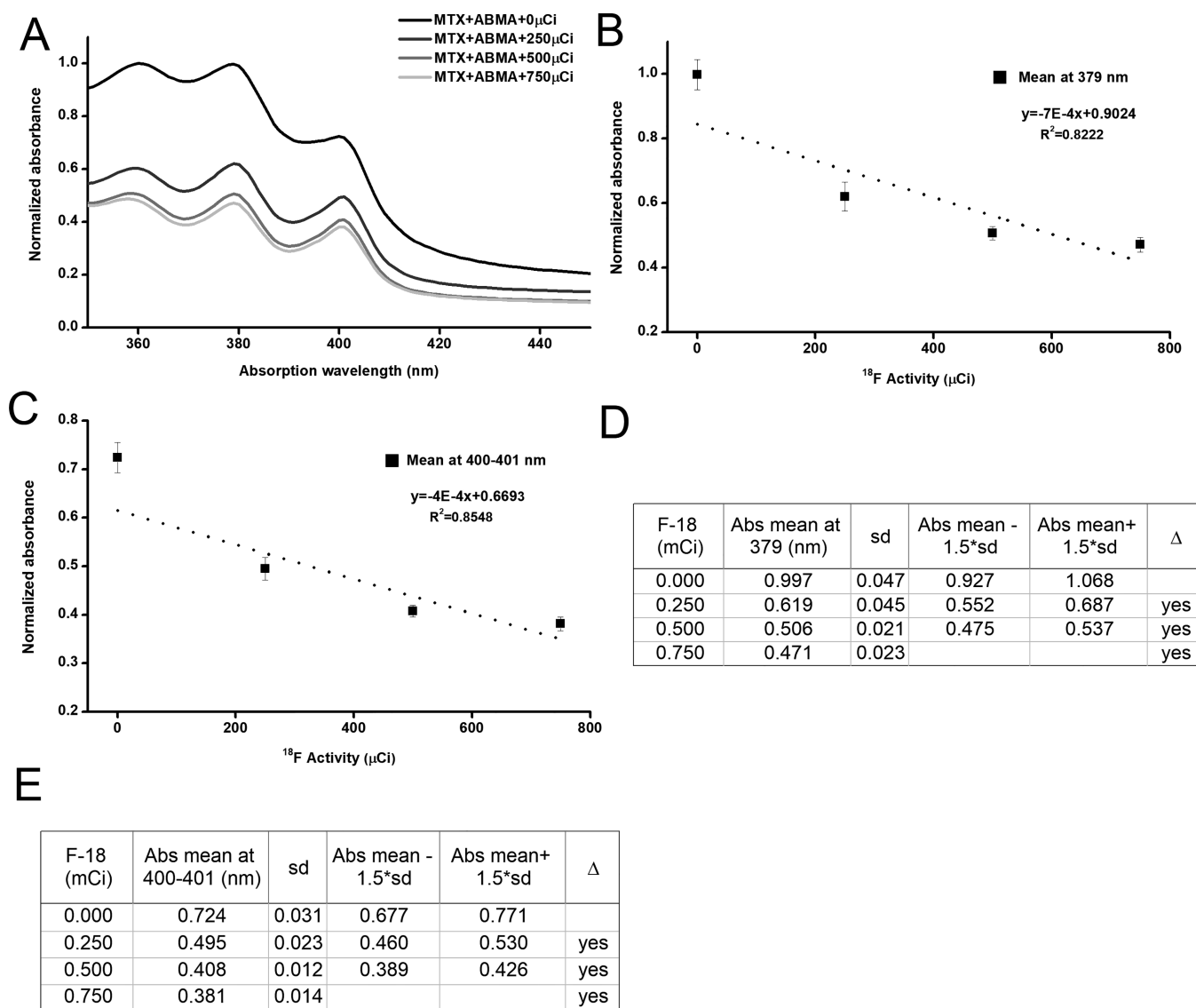
Figure 6. Variation of the absorption spectrum, in the range of 350−450 nm, of solutions of ABMA (200 μM) + MTX (200 μM) in the presence of increasing activities of ^{18}F-FDG (A). The behavior of the normalized absorbance of the ABMA+MTX solution at 379 nm (B) and at 400−401 nm (C) in the presence of increasing activities of ^{18}F-FDG, whose values are detailed in (D) and (E), respectively.
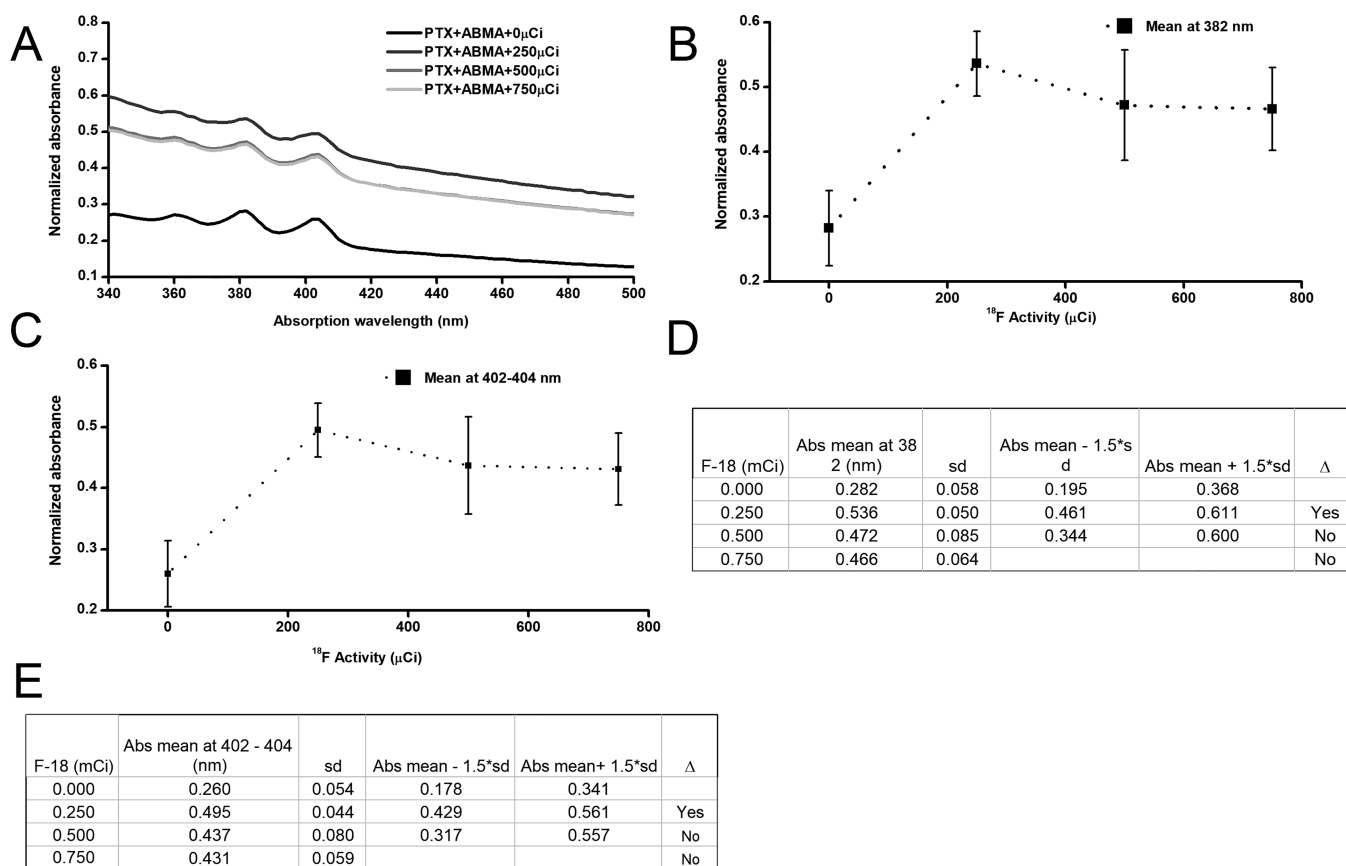
tionally to the rate of cellular glycolysis.[36] Both types of transporters are overexpressed on the surface of a wide range of tumor cells, providing the potential for easy introduction of MTX and ^{18}F-FDG into tumor cells to produce intracellular ROS.

There are controversial criteria about the mechanism of cytotoxicity when CR is used to induce a photodynamic effect. Some authors consider that the cytotoxicity is not due to ROS production by PS excited with CR but to alternative mechanisms caused by ionizing radiation in conjunction with Cerenkov photons.[9,37] However, there is evidence of the intracellular production of ROS when a PS and a radionuclide that induces CR are co-localized in the tissue.[9]

The CellRox Green reagent was used to verify if the MTX + ^{18}F-FDG combination can produce intracellular ROS. CellRox Green is a fluorogenic sensor that directly measures the presence of ROS in vitro. CellRox Green has a weak natural reduced state fluorescence that changes to bright green when oxidized by ROS.[38] The intensity of the green color is directly proportional to the intracellular concentration of ROS.

Figure 13 shows that the T47D cells treated with MTX + ^{18}F-FDG (c) show a greater intensity of the green color in the nucleus and cytoplasm than the cells of the control group (a) and the cells of the group treated only with MTX (b). These results confirm that MTX can produce intracellular ROS (mainly ^{1}O$_2$ according to previous results) because it can be photoactivated with CR from ^{18}F-FDG. The figure clearly shows that ROS production in cells treated with MTX alone (b) is much lower than in cells treated with MTX + ^{18}F-FDG (c). The production of ROS by MTX alone in the cell environment has been reported, and it is associated to its anti-inflammatory and immunosuppressing effect.[39,40]

Cell Viability. To verify if ROS production for the MTX + ^{18}F-FDG system is sufficient to induce appreciable cytotoxicity, a cell viability assay was performed with T47D cells. Colorimetry was used with tetrazolium salts (XTT).[41] The results indicate (Figure 14) that the addition of ^{18}F-FDG activities in the range 15 (0.56 MBq)−100 μCi (3.7 MBq) does not produce appreciable effects on cell viability, which remains without significant variation ($p > 0.05$) around 100%.

F-18 (mCi)	Abs mean at 382 (nm)	sd	Abs mean - 1.5*sd	Abs mean + 1.5*sd	Δ
0.000	0.282	0.058	0.195	0.368	
0.250	0.536	0.050	0.461	0.611	Yes
0.500	0.472	0.085	0.344	0.600	No
0.750	0.466	0.064			No

F-18 (mCi)	Abs mean at 402 - 404 (nm)	sd	Abs mean - 1.5*sd	Abs mean+ 1.5*sd	Δ
0.000	0.260	0.054	0.178	0.341	
0.250	0.495	0.044	0.429	0.561	Yes
0.500	0.437	0.080	0.317	0.557	No
0.750	0.431	0.059			No

Figure 7. Variation of the absorption spectrum of ABMA (50 μM) in the presence of PTX (200 μM) and increasing activities of ^{18}F-FDG in the range of 0−800 nm (A). Variation of the normalized absorbance of the ABMA+PTX solution at 382 (B) and at 4020−404 nm (C) in the presence of increasing activities of ^{18}FDG, whose values are detailed in (D) and (E), respectively.
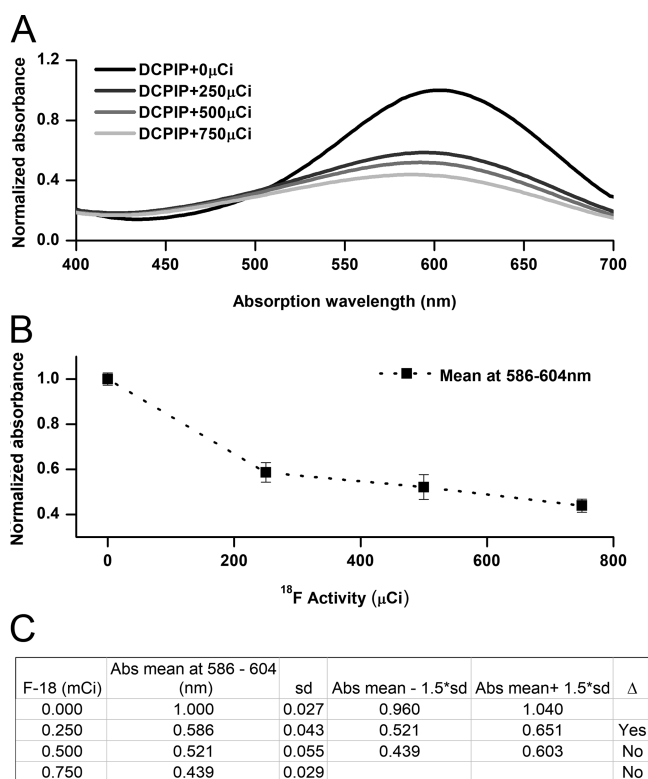
This suggests that ^{18}F-FDG radiation is not capable of causing cytotoxicity on the cell line used, even though it is a radiation-sensitive line.[42] In the presence of 100 nM of MTX, cell viability decreased by around 30% with respect to the control group, which confirms the cytotoxic effect of the chemotherapeutic agent. By adding increasing activities of ^{18}F-FDG in combination with MTX (100 nM), the percentage of viable cells decreases significantly ($p < 0.05$) with increasing ^{18}F-FDG activity, particularly for activities of 50 (1.85 MBq) and 100 μCi (3.7 MBq) of ^{18}F-FDG. The combination of 100 μCi (3.7 MBq) of ^{18}F-FDG + 100 nM of MTX produced about 50% of cell death, which corroborates the CMT + PDT synergy that occurs when MTX is irradiated with CR since the radiation of ^{18}F-FDG by itself was not capable of producing a cytotoxic effect. Similar results were obtained by Quintos-Meneses et al.[13] when evaluating the cytotoxic effect induced by DOX excitation with CR from ^{18}F-FDG. These authors found a significant decrease in the viability of T47D cells when using DOX + ^{18}F-FDG compared to the individual effect produced separately by DOX or ^{18}F-FDG.

PDT is mostly known to induce cell death via apoptosis, necrosis, or autophagy depending on the localization of the PS within cancer cells. For example, if the PS is in endoplasmic reticulum (ER), it can induce autophagy, or necrosis when it is on cell membrane. The presence of PS in nucleus, ER, and mitochondria can induce apoptosis.[1] According to the Nomenclature Committee on Cell Death (NCCD), more cell death mechanisms have been proposed: mitotic catastrophe, piroptosis, parthanatos, necroptosis, and ferroptosis.[43]

However, these mechanisms have been poorly evaluated in PDT. Considering that MTX accumulates in the cell cytoplasm and induces apoptosis[44,45] and that photocytotoxicity under visible light irradiation of PS also produces apoptosis,[46,47] it is expected that apoptosis is strongly involved in the reduction of cell viability induced by MTX + CR (Figure 14). Furthermore, it has been reported that MTX increases the expression of different genes such as BBC3 and BCl3, related with Bcl2, among others.[48] There is evidence that chemo-photodynamic systems downregulate apoptosis-related gene expression in cancer cells such as Bcl2.[3,47] Therefore, it also is expected that MTX + CR induces modulation of cancer-critical genes, related to apoptosis, which could be a strategy to improve therapeutic response.

Our results reaffirm that the use of ^{18}F-FDG CR to obtain a photodynamic effect is an effective approach that contributes to overcoming the difficulties of PDT with external radiation. Additionally, in in vivo experiments greater toxicity is expected since the intensity of CR increases from in vitro studies (refractive index of water, $n = 1.33$), to in vivo studies where the refractive index of biological tissue is higher ($n \approx 1.40$).[10] The use of chemotherapeutic agents with properties similar to PS would increase the efficacy of chemotherapy due to the CMT + PDT synergy. However, to maximize the CMT + PDT effect in vivo, a high accumulation in the target cell of the chemotherapeutic-photosensitizer agent is desire. Although MTX has some specific accumulation in cancer cells due to the overexpression of folate receptor,[49] this specific accumulation can be improved (multivalent effect) using intelligent drug
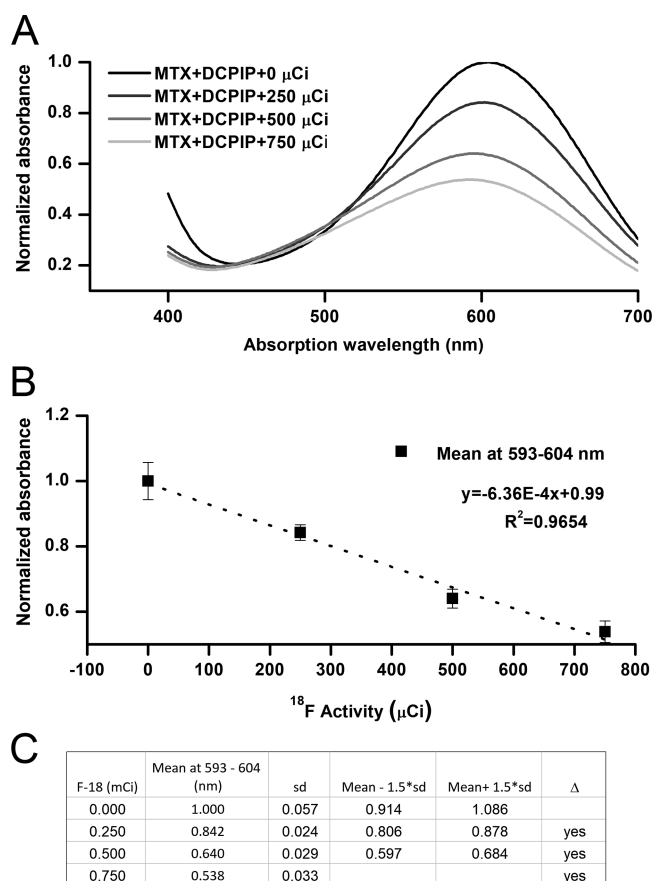
A

B

C

F-18 (mCi)	Abs mean at 586 - 604 (nm)	sd	Abs mean - 1.5*sd	Abs mean+ 1.5*sd	Δ
0.000	1.000	0.027	0.960	1.040	
0.250	0.586	0.043	0.521	0.651	Yes
0.500	0.521	0.055	0.439	0.603	No
0.750	0.439	0.029			No

Figure 8. Irradiation of an aqueous solution of DCPIP (140 μM) with different activities of ^{18}F-FDG. (A) DCPIP absorption spectrum in the 400−700 nm range. (B) Variation of the absorbance of the 586−604 nm band of DCPIP as a function of ^{18}F-FDG activity. (C) Analysis of the variation in the absorbance of the 586−604 nm band of DCPIP as a function of ^{18}F-FDG activity.

delivery systems for transport. Further studies are required to determine an appropriate drug delivery system for this aim.

■ CONCLUSIONS

PTX was not adequate to produce a photodynamic effect with CR from ^{18}F-FDG despite this being theoretically possible. When PTX dissolved in DMSO was irradiated with increasing ^{18}F-FDG activities, the presence of $^1O_2$ and O_2^{*-} was not detected, although the product showed photobleaching, apparently due to mechanisms induced by ionizing radiation and not by photoreaction. MTX, however, produces $^1O_2$ when excited by CR from ^{18}F-FDG in the presence of O_2 while showing high photostability. When MTX + ^{18}FDG was introduced into T47D cells, a much higher intracellular proportion of ROS was observed than when MTX alone was used. This higher intracellular proportion of ROS causes a significant decrease ($p < 0.05$) in cell viability of the combination MTX + ^{18}F-FDG (~50%) compared to MTX (~30%) and ^{18}F-FDG (0%), demonstrating the (i) therapeutic potential of photoactivation with CR and (ii) greater efficacy of CMT + PDT treatment. The use of chemotherapeutic agents already approved for clinical use and with characteristics similar to PS will allow for shortening the evaluation stages of new CMT + PDT systems. The use of ^{18}F-FDG offers the additional advantage of obtaining an image of the treatment site by positron emission tomography (PET), which makes the MTX + ^{18}F-FDG system theragnostic.

A

B

$$y = -6.36E-4x + 0.99$$
$$R^2 = 0.9654$$

C

F-18 (mCi)	Mean at 593 - 604 (nm)	sd	Mean - 1.5*sd	Mean+ 1.5*sd	Δ
0.000	1.000	0.057	0.914	1.086	
0.250	0.842	0.024	0.806	0.878	yes
0.500	0.640	0.029	0.597	0.684	yes
0.750	0.538	0.033			yes

Figure 9. (A) Variation of the absorption spectrum of solutions of DCPIP (140 μM) + MTX (200 μM) in the presence of increasing activities of ^{18}F-FDG in the range of 450−700 nm. (B) Behavior of the normalized absorbance of DCPIP+MTX solution at 593−604 nm in the presence of increasing activities of ^{18}FDG, whose values are detailed in (C).

■ MATERIALS AND METHODS

Reagents and Equipment. The following compounds were used: methotrexate (MTX, Sigma Aldrich), paclitaxel (PTX, Toronto Research Chemicals, TRC), 9,10-anthracene-diyl-bis(methylene) dimalonic acid (ABMA, Sigma Aldrich), 2,6-dichlorophenolindophenol (DCPIP, Sigma Aldrich), ^{18}F-FDG (UNAM, Mexico), Roswell Park Memorial Institute medium (RPMI, 1640, Sigma Aldrich), bovine fetal serum (BFS, Gibco), amphotericin B (Sigma Aldrich), penicillin−streptomycin (Gibco), sodium 3′-[1-[(phenylamino)-carbony]-3,4-tetrazolium]-bis(4-methoxy-6-nitro) benzene-sulfonic acid hydrate (XTT kit, Roche), 4′,6-diamidine-2′-phenylindole dihydrochloride (DAPI, Sigma, Aldrich), and CellRox Green (Fisher Scientific).

A GENESYS 50 UV−vis spectrophotometer (Thermo Fisher Scientific) with 2 nm resolution was used with 250 μL quartz cells (1 cm optical path). We also used a UV−vis Epoch microplate reader (Biotek) and an Eclipse fluorescence microscope (Nikon).

Cell Culture. T47D cells (hormone-dependent luminal subtype A human breast cancer), originally obtained from ATCC (Atlanta, GA, USA), were cultured in RPMI medium supplemented with 10% fetal bovine serum (FBS) with 1% antibiotic and antimycotic solution (Sigma-Aldrich). Cell
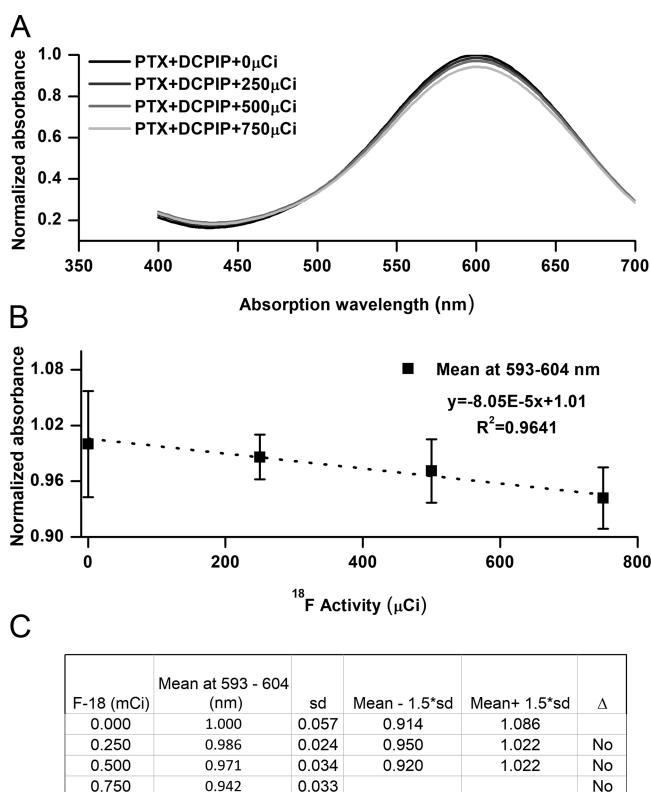
Figure 10. (A) Variation of the absorption spectrum of solutions of DCPIP (140 μM) + PTX (200 μM) in the presence of increasing activities of ^{18}F-FDG in the range of 450−700 nm. (B) Behavior of the normalized absorbance of the DCPIP+PTX solution at 600 nm in the presence of increasing activities of [18]FDG, whose analysis is shown in (C).
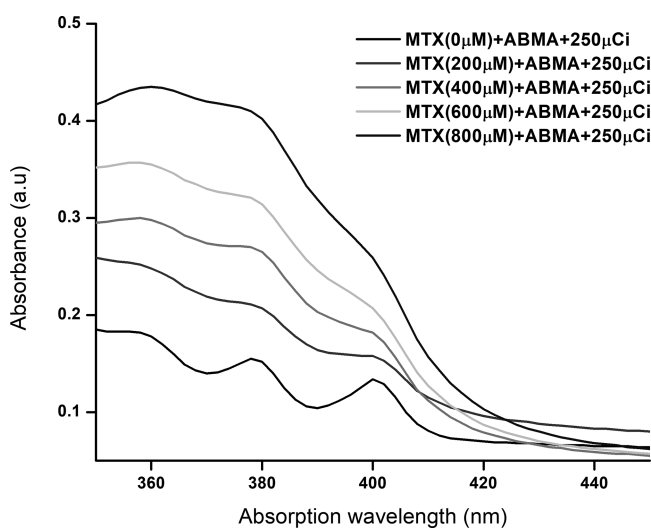
Figure 11. (A) Variation of the absorption spectrum in the range of 350−450 nm of solutions of ABMA (50 μM) + 250 μCi of ^{18}F-FDG in the presence of increasing amounts of MTX.

cultures were incubated at 37 °C with 5% CO_2 and 85% humidity.

Irradiation of MTX, PTX, ABMA, and DCPIP with Increasing Activities of ^{18}F-FDG. MTX: In wells of a 96-well culture plate, sufficient volumes of MTX and ^{18}F-FDG were added, such that in 100 μL, there were 200 μM of MTX and the following ^{18}F-FDG activities: 0, 250, 500, and 750 μCi,

corresponding to 0, 92.5, 18.5, and 27.75 MBq, respectively. The solutions were kept for 24 h in complete darkness. The solutions' UV−vis spectra (300−500 nm) were recorded in an Epoch microplate reader (Biotek).

PTX: Solutions with PTX and ^{18}F-FDG were prepared such that in the final volume of 250 μL, there were 200 μM of PTX and the following ^{18}F-FDG activities: 0, 250, 500, and 750 μCi, corresponding to 0, 92.5, 18.5, and 27.75 MBq, respectively. The solutions were kept for 24 h in complete darkness, and subsequently, the UV−vis spectra (200−350 nm) were recorded in quartz cuvettes using a GENESYS 50 UV−vis spectrophotometer (Thermo Fisher Scientific).

ABMA: Sufficient volumes of ABMA and ^{18}F-FDG were added to wells of a 96-well culture plate such that in the final volume of 100 μL, there were 50 μM ABMA and the following ^{18}F-FDG activities: 0, 250, 500, and 750 μCi, corresponding to 0, 92.5, 18.5, 27.75 MBq, respectively. The solutions were kept for 24 h in complete darkness, and subsequently, the UV−vis spectra (350−450 nm) of the solutions contained in the wells were recorded in the Epoch microplate reader (Biotek).

DCPIP: Sufficient volumes of DCPIP and ^{18}F-FDG were added to wells of a 96-well culture plate such that in the final volume of 100 μL, there were 140 μM of DCPIP and the following ^{18}F-FDG activities: 0, 250, 500, and 750 μCi, corresponding to 0, 92.5, 18.5, and 27.75 MBq, respectively. The solutions were kept for 24 h in complete darkness, and subsequently, the UV−vis spectra (400−700 nm) of the solutions were recorded in the Epoch microplate reader (Biotek).

Spectrophotometric Determination of $^1O_2$ and O_2^{*-} in Solutions of MTX and PTX Irradiated with Increasing Activities of ^{18}F-FDG. *Determination of $^1O_2$.* In wells of a 96-well culture plate, sufficient volumes of MTX or PTX, ABMA, and ^{18}F-FDG were added, such that in 100 μL, there were 200 μM of MTX or PTX, 50 μM of ABMA and the following ^{18}F-FDG activities: 0, 250, 500, and 750 μCi, corresponding to 0, 92.5, 18.5, and 27.75 MBq, respectively. Three replicates for each combination were prepared. The solutions were kept for 24 h in complete darkness. The UV−vis spectrum from 350 to 500 nm was recorded in an Epoch microplate reader (Biotek). To determine the production of $^1O_2$, the shifts and intensities in the absorption bands of ABMA were analyzed and compared with the control solution (ABMA + MTX/PTX + 0 μCi of ^{18}F-FDG).

Determination of O_2^{*-}. In wells of a 96-well culture plate, sufficient volumes of MTX or PTX, ABMA, and 1[8]F-FDG were added, such that in 100 μL, there were 200 μM of MTX or PTX, 140 μM of DCPIP and the following ^{18}F-FDG activities: 0, 250, 500, and 750 μCi, corresponding to 0, 92.5, 18.5, and 27.75 MBq, respectively. Three replicates for each combination were prepared. The solutions were incubated for 24 h in complete darkness. The UV−vis spectrum from 400 to 700 nm was recorded in an Epoch microplate reader (Biotek). To determine the production of O_2^{*-}, the shifts and intensities in the absorption bands of DCPIP were analyzed and compared with the control solution containing (DCPIP + MTX/PTX + 0 μCi of ^{18}F-FDG).

Spectrophotometric Determination of $^1O_2$ and O_2^{*-} in Solutions with Increasing MTX Concentration and Irradiated with ^{18}F-FDG. Determination of $^1O_2$. In wells of a 96-well culture plate, sufficient volumes of MTX, ABMA, and ^{18}F-FDG were added, such that in 100 μL, there were 50 μM of ABMA, 250 μCi (92.5 MBq) ^{18}F-FDG, and 0, 200, 400,
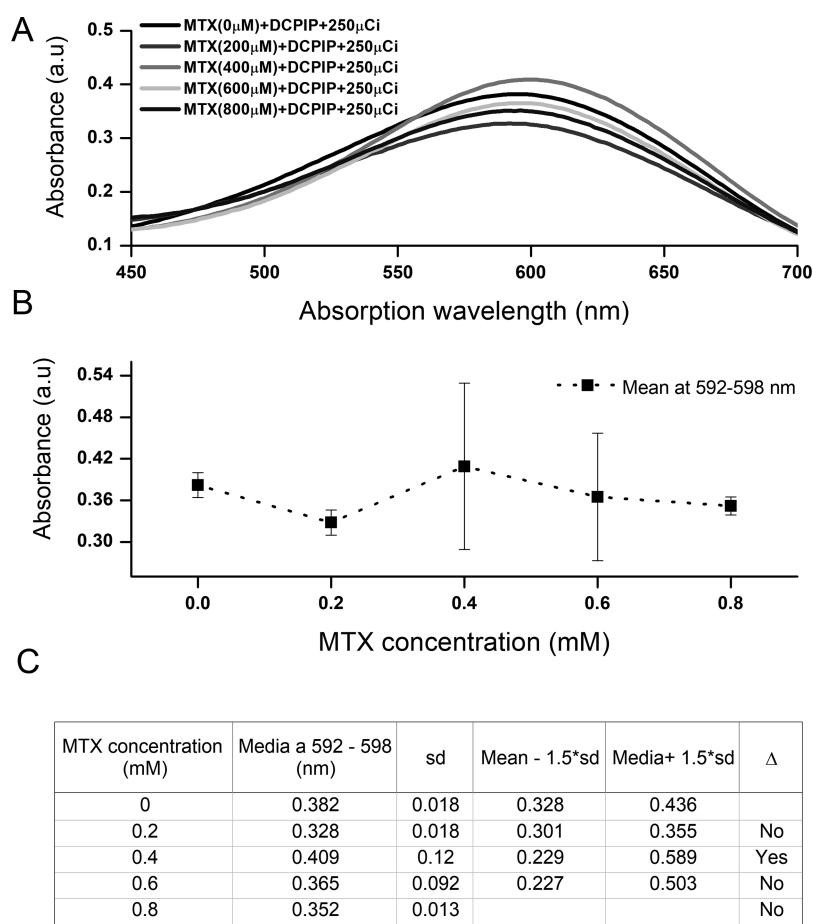
Figure 12. (A) Variation of the absorption spectrum in the range of 450−700 nm of solutions of DCPIP (140 μM) + 250 μCi of ^{18}F-FDG in the presence of increasing amounts of MTX. (B) Behavior of the absorbance at 592−598 nm of the solutions of DCPIP +^{18}F-FDG depending on the concentration of MTX. (C) Analysis of graph (B).

MTX concentration (mM)	Media a 592 - 598 (nm)	sd	Mean - 1.5*sd	Media+ 1.5*sd	Δ
0	0.382	0.018	0.328	0.436	
0.2	0.328	0.018	0.301	0.355	No
0.4	0.409	0.12	0.229	0.589	Yes
0.6	0.365	0.092	0.227	0.503	No
0.8	0.352	0.013			No

600, and 800 μM MTX. Three replicates for each combination were prepared. The solutions were kept for 24 h in complete darkness. The UV−vis spectrum from 350 to 500 nm was recorded in an Epoch microplate reader (Biotek). To determine the production of $^1O_2$, the shifts and intensities in the absorption bands of ABMA were analyzed and compared with the control solution (ABMA +0 μM MTX + 250 μCi of ^{18}F-FDG).

Determination of $O_2{*}^{-}$. In wells of a 96-well culture plate, sufficient volumes of MTX, DCPIP, and ^{18}F-FDG were added, such that in 100 μL, there were 140 μM of DCPIP, 250 μCi (92.5 MBq) ^{18}F-FDG, and 0, 200, 400, 600, and 800 μM MTX. Three replicates for each combination were prepared. The solutions were kept for 24 h in complete darkness. The UV−vis spectrum from 400 to 700 nm was recorded in an Epoch microplate reader (Biotek). To determine the production of $O_2{*}^{-}$, the shifts and intensities in the absorption bands of DCPIP were analyzed and compared with the control solution (DCPIP +0 μM MTX + 250 μCi of ^{18}F-FDG).

Intracellular Evaluation of ROS. To assess intracellular ROS production, 2.5×10^5 cells were seeded in chamber slides with RPMI medium supplemented with 10% FBS and 1% antibiotics and incubated in CO_2 at 5 and 85% humidity for 24 h. Subsequently, cells on each slide were treated for 1 h as follows: slide 1:1× PBS pH 7.2−7.6 (control); slide 2: 100 μM MTX solution; slide 3: 100 μM MTX + 50 μCi (18.5 MBq) ^{18}F-FDG solution. After incubation, CellRox Green reagent

(485/520 nm) was added at a concentration of 5 μM with an incubation time of 30 min at 37 °C. The medium was decanted and washed three times with 1× PBS (pH 7.2−7.6). Samples were fixed with 2% paraformaldehyde for 15 min and washed again with 1× PBS. The fluorescent DAPI marker (VECTA-SHIELD Antifade Mounting Medium with DAPI) was added, and they were covered with a coverslip, incubating for 5 min in the dark at 37 °C before acquiring images in the Eclipse fluorescence microscope (Nikon).

Cell Viability Assay. For this assay, T47D cells were seeded in a 96-well plate at a density of 2.5×10^4 cells/well, which were incubated in 5% CO_2 and 85% humidity for 24 h before treatment ($n = 4$). The cells were incubated with MTX (100 nM) and exposed to different activities of ^{18}F-FDG: 0, 15, 25, 50, and 100 μCi, corresponding to 0, 0.555, 0.925, 1.850, and 3.700 MBq, respectively. At the end of the treatment, the medium was removed, and the cells were washed twice with sterile 1× PBS. Next, 1× PBS (100 μL) was placed in each well and 50 μL of the XTT reaction mixture (sodium 3′-[1-[(phenylamino)-carbony]-3,4-tetrazolium]-bis(4-methoxy-6-nitro)benzene-sulfonic acid hydrate). After 24 h, viability was measured by absorbance in the UV−vis Epoch microplate reader (Biotek).

Statistical Analysis. The comparison of the different treatments was carried out using univariate ANOVA. Where necessary, a Student's t-test was performed. Values of $\alpha < 0.05$ for the two-tailed test were considered significant.
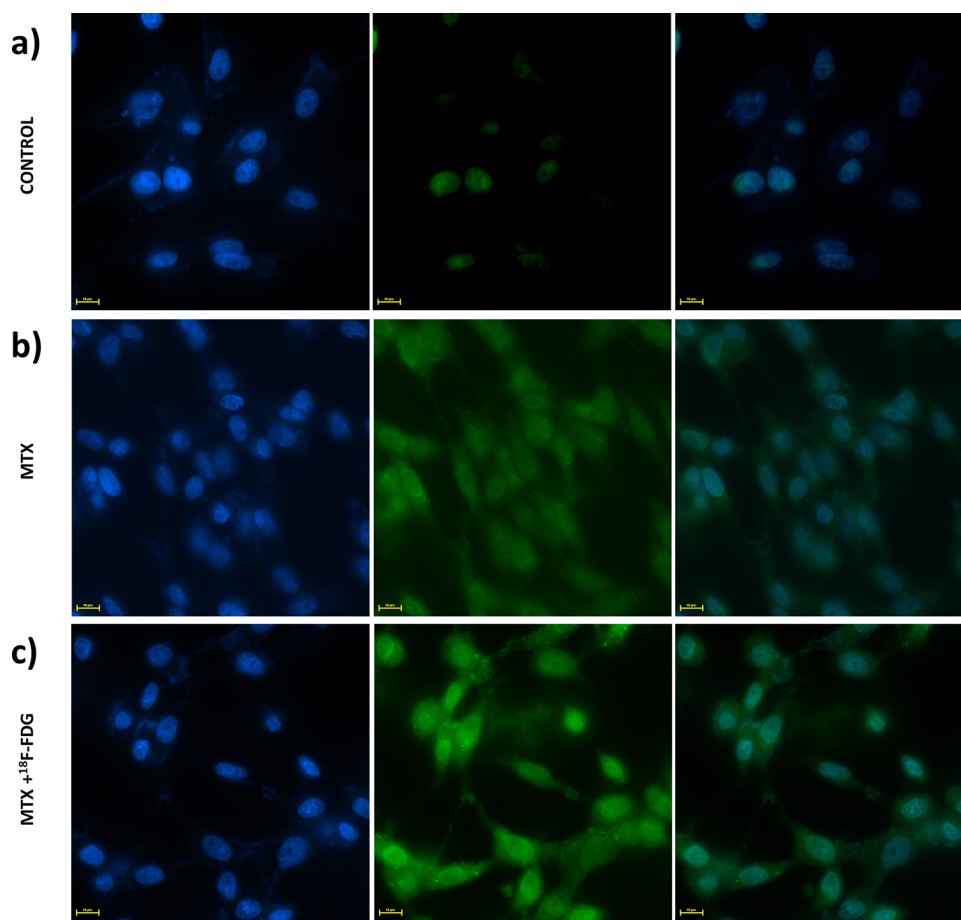
Figure 13. Intracellular production of ROS (a) control group; (b) cells treated with MTX; (c) cells treated with MTX + ^{18}F-FDG.
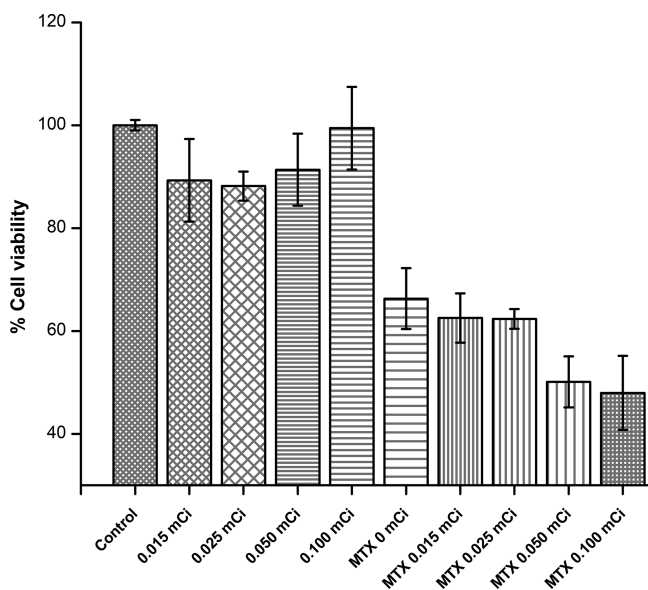
Figure 14. Viability of T47D cells in the presence of MTX and ^{18}F-FDG solutions.

■ AUTHOR INFORMATION

Corresponding Authors

Liliana Aranda-Lara − *Laboratorio de Investigación Teranóstica. Facultad de Medicina, Universidad Autónoma del Estado de México, Toluca 50180 Estado de México, México*; Email: larandal@uaemex.mx

Keila Isaac-Olivé − *Laboratorio de Investigación Teranóstica. Facultad de Medicina, Universidad Autónoma del Estado de México, Toluca 50180 Estado de México, México*; orcid.org/0000-0003-4388-3811; Email: kisaaco@uaemex.mx

Authors

Uriel Gallaga-González − *Laboratorio de Investigación Teranóstica. Facultad de Medicina, Universidad Autónoma del Estado de México, Toluca 50180 Estado de México, México*

Enrique Morales-Avila − *Laboratorio de Toxicología y Farmacia, Facultad de Química, Universidad Autónoma del Estado de México, Toluca 50120 Estado de México, México*

Eugenio Torres-García − *Laboratorio de Dosimetría y Simulación Monte Carlo, Facultad de Medicina, Universidad Autónoma del Estado de México, Toluca 50180 Estado de México, México*

José A. Estrada − *Laboratorio de Neuroquímica, Facultad de Medicina, Universidad Autónoma del Estado de México, Toluca 50180 Estado de México, México*

Luis Enrique Díaz-Sánchez − *Facultad de Ciencias, Universidad Autónoma del Estado de México, Toluca 50120 Estado de México, México*

German Izquierdo − *Facultad de Ciencias, Universidad Autónoma del Estado de México, Toluca 50120 Estado de México, México*

Complete contact information is available at:
https://pubs.acs.org/10.1021/acsomega.2c02153

Author Contributions

Conceptualization was done by L.A.-L., K.I.-O., and E.M.-A.; methodology was done by L.A.-L., K.I.-O., E.T.-G., and J.A.E.; investigation was done by U.G.-G., L.E.D-S, G.I; formal analysis was done by L.A.-L., K.I.-O., E.M.-A., and G.I; writing of the original draft preparation was done by U.G.-G.; validation was done by L.A.-L., K.I.-O., and E.M.-A.; resource gathering was done by J.A.E., E.T.-G., and L.E.D.-S,; funding acquisition was done by L.A.-L.; and writing of the review and editing were done by G.I., E.T.-G., and L.E.D.-S. All authors have read and agreed to the published version of the manuscript.

Notes

The authors declare no competing financial interest.

■ REFERENCES

(1) Mokoena, D. R.; George, B. P.; Abrahamse, H. Photodynamic Therapy Induced Cell Death Mechanisms in Breast Cancer. *Int. J. Mol. Sci.* **2021**, *22*, 10506.

(2) Chen, Y.; Gao, Y.; Li, Y.; Wang, K.; Zhu, J. Synergistic Chemo-Photodynamic Therapy Mediated by Light-Activated ROS-Degradable Nanocarriers. *J. Mater. Chem. B* **2019**, *7*, 460−468.

(3) Sun, X.-Y.; Liu, M.-C.; Chen, X.-L.; Lin, H.-C.; Liu, B.; Peng, Y.-B.; Zhang, L.-Y.; Shen, J.-L.; Zhao, P. A Dual-Targeted Nucleic Acid Moiety Decorated SPION Nanoparticles for Chemo-Photodynamic Synergistic Therapy. *J. Lumin.* **2019**, *209*, 387−397.

(4) Dos Santos, A. F.; De Almeida, D. R. Q.; Terra, L. F.; Baptista, M. S.; Labriola, L. Photodynamic Therapy in Cancer Treatment - an Update Review. *J. Cancer Metastasis Treat.* **2019**, *2019*, 25.

(5) Algorri, J. F.; Ochoa, M.; Roldán-Varona, P.; Rodríguez-Cobo, L.; López-Higuera, J. M. Photodynamic Therapy: A Compendium of Latest Reviews. *Cancers (Basel).* **2021**, *13*, 4447.

(6) Krajczewski, J.; Rucińska, K.; Townley, H. E.; Kudelski, A. *Role of Various Nanoparticles in Photodynamic Therapy and Detection Methods of Singlet Oxygen*; Elsevier B.V., 2019; Vol. 26, pp. 162−178, DOI: 10.1016/j.pdpdt.2019.03.016.

(7) Abrahamse, H.; Hamblin, M. R. New Photosensitizers for Photodynamic Therapy. *Biochem. J.* **2016**, *473*, 347−364.

(8) Spinelli, A. E.; Boschi, F. Photodynamic Therapy Using Cerenkov and Radioluminescence Light. *Front. Phys.* **2021**, *9*, xxx.

(9) Daouk, J.; Dhaini, B.; Petit, J.; Frochot, C.; Barberi-Heyob, M.; Schohn, H. Can Cerenkov Light Really Induce an Effective Photodynamic Therapy? *Radiation* **2021**, *1*, 5−17.

(10) Jiménez-Mancilla, N. P.; Aranda-Lara, L.; Morales-Ávila, E.; Camacho-López, M. A.; Ocampo-García, B. E.; Torres-García, E.; Estrada-Guadarrama, J. A.; Santos-Cuevas, C. L.; Isaac-Olivé, K. Electron Transfer Reactions in Rhodamine: Potential Use in Photodynamic Therapy. *J. Photochem. Photobiol., A* **2021**, *409*, No. 113131.

(11) Hartl, B. A.; Hirschberg, H.; Marcu, L.; Cherry, S. R. Activating Photodynamic Therapy in Vitro with Cerenkov Radiation Generated from Yttrium-90. *J. Environ. Pathol. Toxicol. Oncol.* **2016**, *35*, 185−192.

(12) Nakamura, Y.; Nagaya, T.; Sato, K.; Okuyama, S.; Ogata, F.; Wong, K.; Adler, S.; Choyke, P. L.; Kobayashi, H. Cerenkov Radiation−Induced Photoimmunotherapy with 18 F-FDG. *J. Nucl. Med.* **2017**, *58*, 1395−1400.

(13) Quintos-Meneses, H. A.; Aranda-Lara, L.; Morales-Ávila, E.; Torres-García, E.; Camacho-López, M. Á.; Sánchez-Holguín, M.; Luna-Gutiérrez, M. A.; Ramírez-Durán, N.; Isaac-Olivé, K. In Vitro Irradiation of Doxorubicin with 18F-FDG Cerenkov Radiation and Its Potential Application as a Theragnostic System. *J. Photochem. Photobiol. B Biol.* **2020**, *210*, No. 111961.

(14) Shaffer, T. M.; Pratt, E. C.; Grimm, J. Utilizing the Power of Cerenkov Light with Nanotechnology. *Nat. Nanotechnol.* **2017**, 106.

(15) Jiménez-Mancilla, N. P.; Isaac-Olivé, K.; Torres-García, E.; Camacho-López, M. A.; Ramírez-Nava, G. J.; Mendoza-Nava, H. J. Theoretical and Experimental Characterization of Emission and Transmission Spectra of Cerenkov Radiation Generated by 177Lu in Tissue. *J. Biomed. Opt.* **2019**, *24*, 1.

(16) Motlagh, N. S. H.; Parvin, P.; Ghasemi, F.; Atyabi, F. Fluorescence Properties of Several Chemotherapy Drugs: Doxorubicin, Paclitaxel and Bleomycin. *Biomed. Opt. Express* **2016**, *7*, 2400.

(17) Pascu, M. L.; Staicu, A.; Voicu, L.; Brezeanu, M.; Carstocea, B.; Pascu, R.; Gazdaru, D. Methotrexate as a Photosensitiser. *Anticancer Res.* **2004**, *24*, 2925−2930.

(18) Quintos-Meneses, H. A.; Aranda-Lara, L.; Morales-Ávila, E.; Ocampo-García, B.; Contreras, I.; Ramírez-Nava, G. J.; Santos-Cuevas, C. L.; Estrada, J. A.; Luna-Gutiérrez, M. A.; Ferro-Flores, G.; Camacho-López, M. A.; Torres-García, E.; Ramírez-Durán, N.; Isaac-Olivé, K. A Multimodal Theranostic System Prepared from High-Density Lipoprotein Carrier of Doxorubicin and (177)Lu. *J. Biomed. Nanotechnol.* **2021**, *17*, 2125−2141.

(19) Jahn, B.; Jonasson, N. S. W.; Hu, H.; Singer, H.; Pol, A.; Good, N. M.; den Camp, H. J. M. O.; Martinez-Gomez, N. C.; Daumann, L. J. Understanding the Chemistry of the Artificial Electron Acceptors PES, PMS, DCPIP and Wurster's Blue in Methanol Dehydrogenase Assays. *J. Biol. Inorg. Chem.* **2020**, *25*, 199−212.

(20) Malcomson, T.; Paterson, M. J. Theoretical Determination of Two-Photon Absorption in Biologically Relevant Pterin Derivatives. *Photochem. Photobiol. Sci.* **2020**, *19*, 1538−1547.

(21) Pascu, M.-L.; Mogos, I.; Enescu, M.; Staicu, A.; Truica, S.; Voicu, L.; Gazdaru, D. M.; Pascu, M. O.; Radu, A. Optical Properties of Cytostatic Drugs Used in Cancer Treatment. In *Laser Florence 2000: A Window on the Laser Medicine World*; Longo, L., Hofstetter, A. G., Pascu, M.-L., Waidelich, W. R. A., Eds.; SPIE, 2001; Vol. *4606*, pp. 66−71, DOI: 10.1117/12.446699.

(22) Guichard, N.; Guillarme, D.; Bonnabry, P.; Fleury-Souverain, S. Antineoplastic Drugs and Their Analysis: A State of the Art Review. *Analyst* **2017**, *142*, 2273−2321.

(23) Karami, F.; Ranjbar, S.; Ghasemi, Y.; Negahdaripour, M. Analytical Methodologies for Determination of Methotrexate and Its Metabolites in Pharmaceutical, Biological and Environmental Samples. *J. Pharm. Anal.* **2019**, *9*, 373−391.

(24) Centelles, J. J.; Imperial, S. Paclitaxel: Descubrimiento, Propiedades y Uso Clinico. *Ambito Farm.* **2010**, *29*, 68−75.

(25) Torres-García, E.; Torres-Velazquez, H.; Díaz-Sánchez, L. E.; Aranda-Lara, L.; Isaac-Olivé, K. Determination of experimental Cherenkov spectrum (200−1050 nm) of ^{18}F and its implications on optical dosimetry: murine model. *Radiat. Eff. Defects Solids* **2022**, 1.

(26) Demchenko, A. P. Photobleaching of Organic Fluorophores: Quantitative Characterization, Mechanisms, Protection. *Methods Appl. Fluoresc.* **2020**, *8*, 22001.

(27) Zheng, Q.; Jockusch, S.; Zhou, Z.; Blanchard, S. C. The Contribution of Reactive Oxygen Species to the Photobleaching of Organic Fluorophores. *Photochem. Photobiol.* **2014**, *90*, 448−454.

(28) Getoff, N.; Solar, S.; Richter, U.-B.; Haenel, M. W. Pulse Radiolysis of Pyrene in Aprotic Polar Organic Solvents: Simultaneous Formation of Pyrene Radical Cations and Radical Anions. *Radiat. Phys. Chem.* **2003**, *66*, 207−214.

(29) Alkhuraiji, T. S. Advanced Oxidation Process Based on Water Radiolysis to Degrade and Mineralize Diclofenac in Aqueous Solutions. *Sci. Total Environ.* **2019**, *688*, 708−717.

(30) Mastropaolo, D.; Camerman, A.; Luo, Y.; Brayer, G. D.; Camerman, N. Crystal and Molecular Structure of Paclitaxel (Taxol). *Proc. Natl. Acad. Sci. U. S. A.* **1995**, *92*, 6920−6924.

(31) Yin, H.; Wang, M.; Tan, L.-S.; Chiang, L. Y. Synthesis and Intramolecular Energy- and Electron-Transfer of 3D-Conformeric Tris(Fluorenyl-[60]Fullerenylfluorene) Derivatives. *Molecules* **2019**, *24*, 3337.

(32) Ohsawa, I.; Ishikawa, M.; Takahashi, K.; Watanabe, M.; Nishimaki, K.; Yamagata, K.; Katsura, K.-I.; Katayama, Y.; Asoh, S.; Ohta, S. Hydrogen Acts as a Therapeutic Antioxidant by Selectively Reducing Cytotoxic Oxygen Radicals. *Nat. Med.* **2007**, *13*, 688−694.

(33) Conti, M.; Eriksson, L. Physics of Pure and Non-Pure Positron Emitters for PET: A Review and a Discussion. *EJNMMI Phys.* **2016**, *3*, 8.

(34) Friedman, B.; Cronstein, B. Methotrexate Mechanism in Treatment of Rheumatoid Arthritis. *Jt., Bone, Spine* **2019**, *86*, 301−307.

(35) Nogueira, E.; Sárria, M. P.; Azoia, N. G.; Antunes, E.; Loureiro, A.; Guimarães, D.; Noro, J.; Rollett, A.; Guebitz, G.; Cavaco-Paulo, A. Internalization of Methotrexate Conjugates by Folate Receptor-α. *Biochemistry* **2018**, *57*, 6780−6786.

(36) Rahman, W. T.; Wale, D. J.; Viglianti, B. L.; Townsend, D. M.; Manganaro, M. S.; Gross, M. D.; Wong, K. K.; Rubello, D. The Impact of Infection and Inflammation in Oncologic 18F-FDG PET/CT Imaging. *Biomed. Pharmacother.* **2019**, *117*, No. 109168.

(37) Klein, J. S.; Sun, C.; Pratx, G. Radioluminescence in Biomedicine: Physics, Applications, and Models. *Phys. Med. Biol.* **2019**, No. 04TR01.

(38) Korga, A.; Ostrowska, M.; Jozefczyk, A.; Iwan, M.; Wojcik, R.; Zgorka, G.; Herbet, M.; Vilarrubla, G. G.; Dudka, J. Apigenin and Hesperidin Augment the Toxic Effect of Doxorubicin against HepG2 Cells. *BMC Pharmacol. Toxicol.* **2019**, *20*, 22.

(39) Huang, C.-C.; Hsu, P.-C.; Hung, Y.-C.; Liao, Y.-F.; Liu, C.-C.; Hour, C.-T.; Kao, M.-C.; Tsay, G. J.; Hung, H.-C.; Liu, G. Y. Ornithine Decarboxylase Prevents Methotrexate-Induced Apoptosis by Reducing Intracellular Reactive Oxygen Species Production. *Apoptosis* **2005**, *10*, 895−907.

(40) Phillips, D. C.; Woollard, K. J.; Griffiths, H. R. The Anti-Inflammatory Actions of Methotrexate Are Critically Dependent upon the Production of Reactive Oxygen Species. *Br. J. Pharmacol.* **2003**, *138*, 501−511.

(41) Roehm, N. W.; Rodgers, G. H.; Hatfield, S. M.; Glasebrook, A. L. An Improved Colorimetric Assay for Cell Proliferation and Viability Utilizing the Tetrazolium Salt XTT. *J. Immunol. Methods* **1991**, *142*, 257−265.

(42) Masoudi-Khoram, N.; Abdolmaleki, P.; Hosseinkhan, N.; Nikoofar, A.; Mowla, S. J.; Monfared, H.; Baldassarre, G. Differential MiRNAs Expression Pattern of Irradiated Breast Cancer Cell Lines Is Correlated with Radiation Sensitivity. *Sci. Rep.* **2020**, *10*, 9054.

(43) Mishchenko, T.; Balalaeva, I.; Gorokhova, A.; Vedunova, M.; Krysko, D. V. Which Cell Death Modality Wins the Contest for Photodynamic Therapy of Cancer? *Cell Death Dis.* **2022**, *13*, 455.

(44) AlBasher, G.; AlKahtane, A. A.; Alarifi, S.; Ali, D.; Alessia, M. S.; Almeer, R. S.; Abdel-Daim, M. M.; Al-Sultan, N. K.; Al-Qahtani, A. A.; Ali, H. Methotrexate-Induced Apoptosis in Human Ovarian Adenocarcinoma SKOV-3 Cells via ROS-Mediated Bax/Bcl-2-Cyt-c Release Cascading. *Onco. Targets. Ther.* **2019**, *12*, 21−30.

(45) Bedoui, Y.; Guillot, X.; Sélambarom, J.; Guiraud, P.; Giry, C.; Jaffar-Bandjee, M. C.; Ralandison, S.; Gasque, P. Methotrexate an Old Drug with New Tricks. *Int. J. Mol. Sci.* **2019**, DOI: 10.3390/ijms20205023.

(46) Sun, X.-Y.; Zhao, P.; Jin, S.; Liu, M.-C.; Wang, X.; Huang, Y.; Cheng, Z.; Yan, S.-Q.; Li, Y.-Y.; Chen, Y.-Q.; et al. Shedding Lights on the Flexible-Armed Porphyrins: Human Telomeric G4 DNA Interaction and Cell Photocytotoxicity Research. *J. Photochem. Photobiol. B Biol.* **2017**, *173*, 606−617.

(47) Agostinis, P.; Buytaert, E.; Breyssens, H.; Hendrickx, N. Regulatory Pathways in Photodynamic Therapy Induced Apoptosis. *Photochem. Photobiol. Sci.* **2004**, *3*, 721.

(48) Spurlock, C. F., III; Aune, Z. T.; Tossberg, J. T.; Collins, P. L.; Aune, J. P.; Huston, J. W., III; Crooke, P. S.; Olsen, N. J.; Aune, T. M. Increased Sensitivity to Apoptosis Induced by Methotrexate Is Mediated by JNK. *Arthritis Rheum.* **2011**, *63*, 2606−2616.

(49) Faria, R.; Sousa, Â.; Neves, A. R.; Queiroz, J. A.; Costa, D. Methotrexate-Plasmid DNA Polyplexes for Cancer Therapy: Characterization, Cancer Cell Targeting Ability and Tuned in Vitro Transfection. *J. Mol. Liq.* **2019**, *292*, No. 111391.